Am J Cancer Res 2015;5(5):1610-1620
www.ajcr.us /ISSN:2156-6976/ajcr0006351

Original Article

Glucose-6-phosphate dehydrogenase and NADPH oxidase 4 control STAT3 activity in melanoma cells through a pathway involving reactive oxygen species, c-SRC and SHP2

Tianchi Cai[1*], Yingmin Kuang[2*], Chunhua Zhang[1,3*], Zheng Zhang[1], Long Chen[1], Bo Li[1], Yuqian Li[1], Yanling Wang[1], Huixin Yang[1], Qiaoqiao Han[1], Yuechun Zhu[1]

[1]Department of Biochemistry and Molecular Biology, Kunming Medical University, Kunming 650500, China; [2]The First Hospital affiliated to Kunming Medical University, Kunming 650032, China; [3]The Maternal and Child Health Hospital of Yunnan Province, Kunming 650051, China. [*]Equal contributors.

Received January 26, 2015; Accepted April 1, 2015; Epub April 15, 2015; Published May 1, 2015

Abstract: Background: Glucose-6-phosphate dehydrogenase (G6PD) participates in glucose utilization by catalysing the first step of the pentose-phosphate pathway in mammalian cells. Previous studies have shown that changes in G6PD levels can promote tumor cell proliferation or apoptosis via the STAT3/5 pathway in a human melanoma xenograft model. G6PD cooperates with NADPH oxidase 4 (NOX4) in the cellular metabolism of reactive oxygen species (ROS) and in maintaining the intracellular redox state. Methods: In this study, the effect of G6PD or NOX4 silencing in the melanoma line A375 was examined in terms of redox state, proto-oncogene tyrosine-protein kinase Src (c-Src) and the tyrosine-specific protein phosphatase SHP2 expression as well as cell cycle progression. Results: The results demonstrate that: (1) Downregulation of cyclin D1 and CDK4 and up-regulation of p53 and p21 occurred in response to silencing of G6PD and NOX4 thus resulting in G1/S cell cycle arrest and inhibition of A375 cell proliferation. (2) The blockade of cell proliferation is primarily due to a reduced DNA-binding activity of STAT3. (3) The DNA-binding activity of STAT3 was regulated by the upstream factors, c-SRC and SHP2. Silencing of NOX4 in A375 cells inhibited c-SRC and SHP2 regulated STAT3 activity. Conclusion: The data are consistent with a novel G6PD-NOX4-NADPH-ROS-c-SRC/SHP2 pathway controlling STAT3 activity in A375 melanoma cells.

Keywords: Glucose-6-phosphate dehydrogenase, STAT3/5, NOX4, c-SRC, SHP2, cyclin D1, CDK4

Introduction

Malignant melanoma derives from the transformation of melanocytes in the skin, mucous membranes, eyes or central nervous system [1]. Although the incidence of melanoma is still relatively low in China, it is on the rise with 20,000 new cases diagnosed each year. Melanoma is highly resistant to chemotherapy and has a poor survival rate. Recent research showed that abnormal intracellular ROS levels are closely related to melanoma development [2]. In response to excessive ultraviolet radiation, normal melanocytes showed an increased level of intracellular ROS, which might lead to DNA damage and dysfunction of transcription factors such as NF-κB, AP-1 and HIF. ROS may also alter normal signalling through the JAK/STAT, MAPK, and PI3K/AKT pathways thus leading to dysregulation of cell proliferation and apoptosis [2].

Glucose 6-phosphate dehydrogenase (G6PD) plays an important role in intermediary metabolism and redox regulation. It catalyses the first step of the pentose phosphate pathway thereby producing the reduced form of the co-enzyme nicotinamide adenine dinucleotide phosphate (NADPH). NADPH is required for a variety of biosynthetic and detoxification reactions [3]. An alternative non-canonical glycolytic pathway is also linked with G6PD in certain organisms and in certain circumstances [4]. Thus, G6PD can be regarded an essential housekeeping enzyme. In humans, variant G6PD alleles have been identified which give rise to enzymes with

varying degrees of impaired activity [5, 6]. G6PD activity is dispensable for pentose synthesis but is essential to protect cells against oxidative stress [3].

Previous studies on the A375 cell line have indicated that G6PD regulates the proliferation of human melanoma cells, but the molecular mechanism involved remained largely unknown [7]. G6PD regenerates NADPH, which is a coenzyme of NADPH oxidases including those containing NOX4 [8]. Both G6PD and NOX4 are thus involved in cellular ROS metabolism and the maintenance of the redox state [9]. NOX4 is the catalytic subunit of a membrane bound NADPH oxidase complex composed of $p47^{phox}$, $p67^{phox}$, $p40^{phox}$, Rac and $p22^{phox}$.

The protein tyrosine kinase c-Src and the protein tyrosine phosphatase SHP2 (PTPN11) play essential roles in cell signalling pathways [10, 11]. The activities of c-Src and SHP2 are closely related to the redox state of cysteines, yet their mechanism of redox regulation has not been fully elucidated. STAT3 is a member of the STAT family (signal transducers and activators of transcription) implicated as a downstream target of ROS-activated JAK2 kinase signalling. Previous research showed that hyperactivation of the STAT3 pathway is intimately linked with melanoma development [12, 13].

In order to explore how G6PD and NOX4 affect the proliferation of human melanoma cells, we employed parental A375 cells (A375-WT) as well as derivatives in which G6PD or NOX4 were knocked down (A375-G6PDΔ and A375-NOX4Δ, respectively). Our study revealed a pathway linking G6PD and NOX4 to STAT3 activity through c-SRC and SHP2. The fundamental insights revealed into this pathway may help us identify novel therapeutic targets for melanoma.

Materials and methods

The short hairpin RNA (shRNA) and lentiviral vector

siRNA oligonucleotides were designed based on the published human G6PD (GenBank accession no. NM_000402) and NOX4 (GenBank accession no. NM_001143836) sequences with Oligo Engine 2.0 software (Seattle, WA). Three siRNA target sequences of G6PD (G6PD sh-RNA-1: 2203 GCCTCAGTGCCACTTGACA 2221; G6PD shRNA-2: 2170 CGTGAGAGAATCTGCCTGT 2188; G6PD shRNA-3: 1869 TTGACCTCAGCTGCACATT 1887) and NOX4 (NOX4 shRNA-1: 471 GGCTAGGATT GTGTCTAAGC 490; NOX4 shRNA-2: 592 CAGGAGAACCAGGAGATTGT 612; NOX4 shRNA-3: 951 GGCTG CTGAAGTATCAAACT 970) were selected, and the controls were randomly designed non-specific DNA sequences. The lentiviral vector, pRNAT-U6.2/Lenti (GenScript, Piscataway, NJ), contains the polymerase III (pol III) promoter, U6.2, to drive siRNA and non-specific dsDNA expression, a neomycin-resistance gene driven by cytomegalovirus (CMV) for establishing stable cell lines, and a coral GFP gene driven by SV-40 for tracking transfection efficiency. Each shRNA was synthesized from a complementary ssDNA template. Each ssDNA contained a *BamH I* restriction site at the 5-end, an siRNA or nonspecific sense sequence, 10 oligonucleotides to form the stem-and-loop structure, an siRNA or nonspecific antisense sequence and a pol III termination sequence (TTTTTT).

Preparation of c-Src inhibitor PP1 and SHP-2 inhibitor PTP IV

c-Src inhibitor PP-1 and SHP-2 inhibitor PTP IV (Santa Cruz Biotechnology, Inc, Dallas, Texas 75220 USA) were dissolved with DMSO respectively, and prepared as stock solutions at 25 mg/mL (88.8 mM) and 10 mg/mL (16.4 mM), respectively. 10 μM PP1 and 5 μM PTP inhibitor IV was used to treat three cell lines of A375, A375-G6PDΔ, A375-NOX4Δ for 48 h, respectively. The untreated group was the control group, in which the redox state of the Cys residue in c-Src and SHP-2, protein expression of c-Src and SHP-2, as well as the enzyme activity was determined.

Transient transfection of A375 cells

A375 human melanoma cells were purchased from the American Type Culture Collection (ATCC; Manassas, VA) and grown in DMEM, supplemented with 10% fetal bovine serum (FBS; Gibco-BRL, Gaithersburg, MD). A375 cells were transfected with Lipofectamine™ 2000 (Invitrogen™, Shanghai, China), and plasmid DNA was purified with a plasmid Miniprep kit (Qiagen, Hilden, Germany). Lipid-DNA complexes were overlaid onto the cells, and cells were incubated at 37°C for 24 to 48 h in a tissue-culture incubator under 5% CO_2. When cells

grew to 90% confluence and transfection efficiency reached 50%-60%, as judged by GFP expression, cells were harvested for real-time PCR analysis of G6PD mRNA levels.

Packaging and producing lentiviral particles

To produce lentiviral particles, the 293T packaging cells were transfected with a mixture of plasmids, including the lentiviral expression vector with siRNA1 (pRNAT-U6.2-G6PD siRNA1) and the viral packaging plasmids, a mixture of pPACK-REV, pPACK-GAG, and pVSV-G (Kangchen, Shanghai, China), according to the manufacturer's instructions.

Transfected cells were harvested when their GFP coexpression reached more than 90%. Culture supernatant containing lentiviral particles was collected and passed through a 0.45 μm polyvinylidene fluoride filter. Next, 293T cells were seeded in a 96-well culture plate (1×10^5 cells/well) and divided into a control group infected by the standard virus solution with a known titer 1×10^8 cfu/L (Kangchen, Shanghai, China) and several test groups of cells infected with the newly harvested lentiviral particles at multiplicity of infection (MOI) of 1, 3, 5, 10 and 20. After infection, cells were observed under a fluorescence microscope for GFP expression to estimate the viral titers.

Real-time PCR analysis

Total RNA was isolated from the transfected cells by using Trizol reagent (Invitrogen™, Shanghai, China). cDNA was synthesized by using Oligo (dT)18 and MMLV reverse transcriptase (Promega, Madison, WI). The forward primer of G6PD (F, 5'-TGAGCCAGAT AGGCTGGAA-3') and the reverse primer (R, 5'-TAACGCAGGCG-ATGTTGTC-3'), NOX4: forward primer: F, 5'-GATGTTGGGCTAGGATTGT-3', R, 5'-TCTGTGAT-CCTCGGAGG TAA-3' and the β-actin primers, a forward primer (F, 5-CCTGTACGCCAACACAG-TGC3) and a reverse primer (R, 5-ATACTC-CTGCTTGCTGATCC3), were synthesized by a domestic company (Shengon, Shanghai, China). The cDNA was 10-fold serially diluted to seven concentrations for the standard curve. PCR was performed by the denaturation step at 94°C for 5 min, followed by 35 cycles of 94°C for 10 s, 57°C for 15 s, and 72°C for 30 s. Fluorescent signals from PCR products were recorded at 85.5°C for 5 s. G6PD and NOX4 mRNA levels were normalized as the ratio of the fluorescence intensity from G6PD and NOX4 to that of β-actin. The siRNA construct (siRNA1 of G6PD and NOX4) that both achieved the highest degree of gene silencing was then used for the selection of the A375 stable cell line.

Western blot analysis

The G6PD and NOX4 gene silencing in the siRNA-transfected cells was determined based on the decrease in G6PD and NOX4 protein expression by Western blot analyses. Total proteins were extracted from the wild-type human melanoma cell line A375, human epidermal melanocytes (HEM), M21 and SK-mel-28 and its G6PD siRNA or NOX4 siRNA stable transfected lines. Protein concentrations were measured using a BCA protein quantity kit (Kangcheng, Shanghai, China). Aliquots of cell lysates containing 50 μg of proteins were separated by a 10% SDS–polyacrylamide gel and transferred to a nitrocellulose membrane. The blot was first blocked with TBST buffer containing 5% skim milk and was then incubated with rabbit antihuman G6PD, NOX4, SPH-2 polyclonal antibody (1:2000; Abcam, Cambridge, UK), c-Src anti-rabbit monoclonal (1:2500) or antihuman β-actin antibody (1:2000; Abcam, Cambridge, UK), rabbit anti-human monoclonal cyclin D1, CDK4, p21, p53 antibody and stat3 and phos-stat3 anti-rabbit human monoclonal antibody (BODESHI, Shanghai, China). After several steps of washing, the blot was further incubated with HRP-linked goat anti-rabbit IgG (Boster, Wuhan, China), HRP-linked antimouse IgG, followed by the detection of the bands using an electrochemiluminescence (ECL) system. The intensity of chemifluorescence signals was analyzed using Image J software (National Institutes of Health, Bethesda, MD), and Cyclin D1, CDK4, p21, p53, G6PD, NOX4, c-Src and SHP-2 protein levels were normalized with those of β-actin.

Flow cytometry analysis for cell cycle

Propidium iodide (PI) staining and flow cytometric (FCM) assays were employed for the evaluation of apoptosis. Equal numbers of cells in suspensions (1×10^6 cells) were washed with PBS three times and fixed with 70% ethanol. An aliquot of 1×10^4 cells was stained with PI for 30 min in the dark and subjected to FCM analysis to establish the DNA content of the cells.

Intracellular ROS measurement by dihydroethidium (DHE)

Determination of intracellular ROS levels A375-WT, A375-G6PDΔ and A375-NOX4Δ cells were

cultured in 96-well plates at a density of 5×10^3 cells/well. 24 h after plating, the culture medium was removed and cells were washed twice with PBS. Fresh medium containing the reagent dihydroethidium (DHE) (Invitrogen™, Shanghai, China) at a final concentration of 10 μM was added, followed by incubation at 37°C in the dark for 20 min. Fluorescence intensities were determined by flow cytometry (excitation: 530 nm, emission: 620 nm) with their survival rate and the changes of a series of oxidative-reductive components.

Redox state of cys residue in c-Src and SHP-2 measured with BIAM labelled SDS-PAGE

1×10^6 cells were added to 0.5 mL of cell lysis buffer containing 20 mM BIAM at room temperature allowing 15 min for the reaction of BIAM labelling with cys sulfhydryl (biotin-conjugated iodoacetamide was purchased from Amersham Biosciences, England, UK). The reaction was stopped by adding β-mercaptoethanol (BME), and the supernate collected after centrifugation at 10,000 rpm for 10 min. Then, 50 μL of the supernate was used for 10% SDS PAGE and membrane transfer. HRP-conjugated streptavidin (2 ng/mL) was added and the sample incubated for 1 h at room temperature. Finally, chemiluminescence was used to detect cells in a reduction state and c-Src and SHP-2, which are oxidized by BIAM after cell lysis.

Intracellular c-Src kinase activity assay

1×10^6 cells for each cell line was taken, according to the protocol of the kit (R&D Systems, Inc. Minneapolis, MN 55413 USA) and the same concentration of protein sample prepared. To each 2 μL of sample, the indicated reagent from the protocol was added, and the combined solution placed in a microplate reader where the absorption value at 0 min and 5 min (wavelength 560 nm) was determined. The definition of one active unit c-Src kinase activity at 30°C, pH 7.5, was the required amount of enzyme to oxidize 1 μmol NADH per min.

Intracellular SHP2 phosphatase activity assay

1×10^6 cells for each cell line was added to the protein lysis buffer that was included in the kit (R&D Systems, Inc. Minneapolis, MN 55413 USA), and the supernate collected. Beads were added to prevent SHP-2 antibody coupling to agarose immunoprecipitation products (Duo-Set_IC Human/Mouse/Rat Active SHP-2, R&D Systems, Inc. Minneapolis, MN, USA) and read at 620 nm twice at 0 min and 5 min.

G6PD activity measurements

G6PD activity was measured by its ability to reduce 1 mM of nicotinamide-adenine dinucleotide phosphate ($NADP^+$) in the presence of glucose 6- phosphate, as previously described [7].

Determination of STAT3 in vitro DNA binding activity

Electrophoretic mobility shift assay (EMSA) was performed using the non-radioactive STAT3 EMSA kit (LightShift® Chemiluminescent EMSA Kit, Thermo Fisher Scientific Inc. Rockford, IL, USA) following the manufacturer's instructions. Briefly, 9 μg nuclear protein was combined with 1 μL binding buffer, 1 μL poly (dI:dC) (dI:dC) and 0.5 μL unlabelled competitor oligonucleotide. The samples were pre-incubated at room temperature for 20 min, and then 0.5 μL of biotin-labelled probe (STAT3 probe sequence: 5'-GAT CCT TCT GGG AAT TCC ATC-3') added. Samples were incubated at room temperature for 20 min and separated on 6.5% non-denaturing polyacrylamide gels, followed by transfer to a membrane. DNA was cross-linking and fixed, and membranes were blocked and incubated with streptavidin-HRP for chemiluminescence detection of STAT3-DNA complexes.

Statistical analyses

SPSS version 19.0 software was used for data statistical analysis. The differences among groups ($n \geq 3$) were analysed using one-way ANOVA and post hoc were compared with Student-Newman-Keuls (SNK) test if equal SD. Rank-sum test was used if different SD. An independent sample *t*-test was used if equal SD. *t*-test was used if equal SD. $P < 0.05$ was considered to be statistically significant.

Results

Expression patterns of G6PD and NOX4 in human epidermal melanocytes and melanoma cells

Messenger RNA and protein expression levels of G6PD and NOX4 were determined in human epidermal melanocytes (HEM) and in the

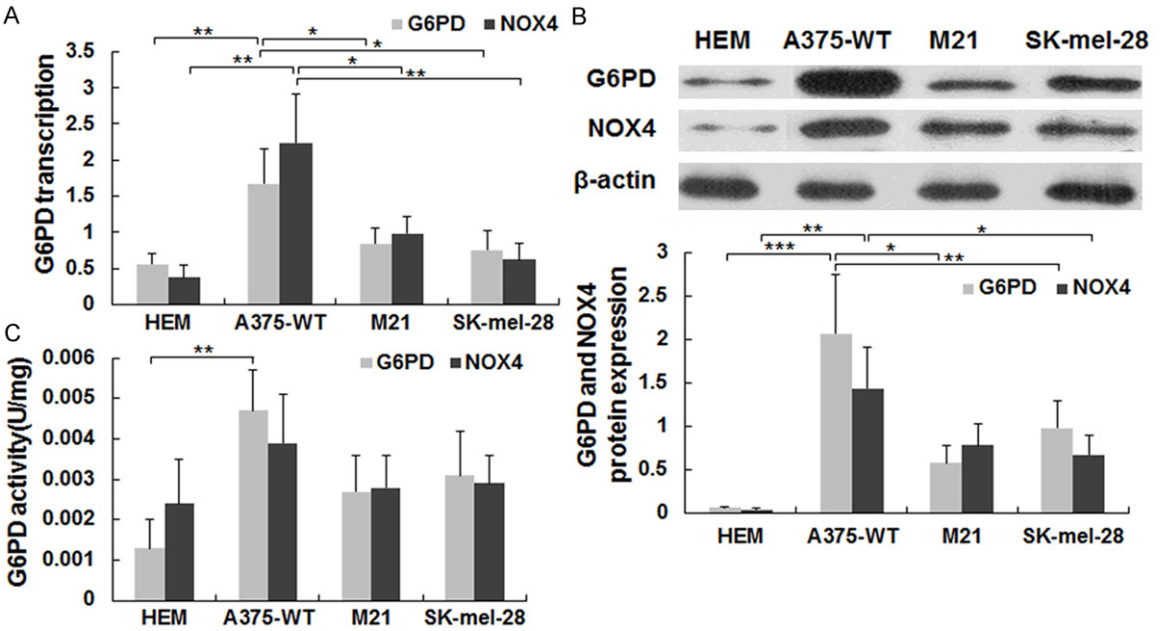

Figure 1. Expression patterns and activities of G6PD and NOX4 in melanoma cells. A. mRNA levels of G6PD and NOX4 in 4 different cells determined by real-time PCR. B. Protein expressions of G6PD and NOX4 in different cells were determined by Western blotting. Data represent average values of 3 experiments and each error bar is the SD. C. G6PD and NOX4 activity in 4 different cells determined by in vitro activity assays (see Methods). Data represent average values of 3 experiments and the error bars are the SD. *P < 0.05, **P < 0.01, ***P < 0.001.

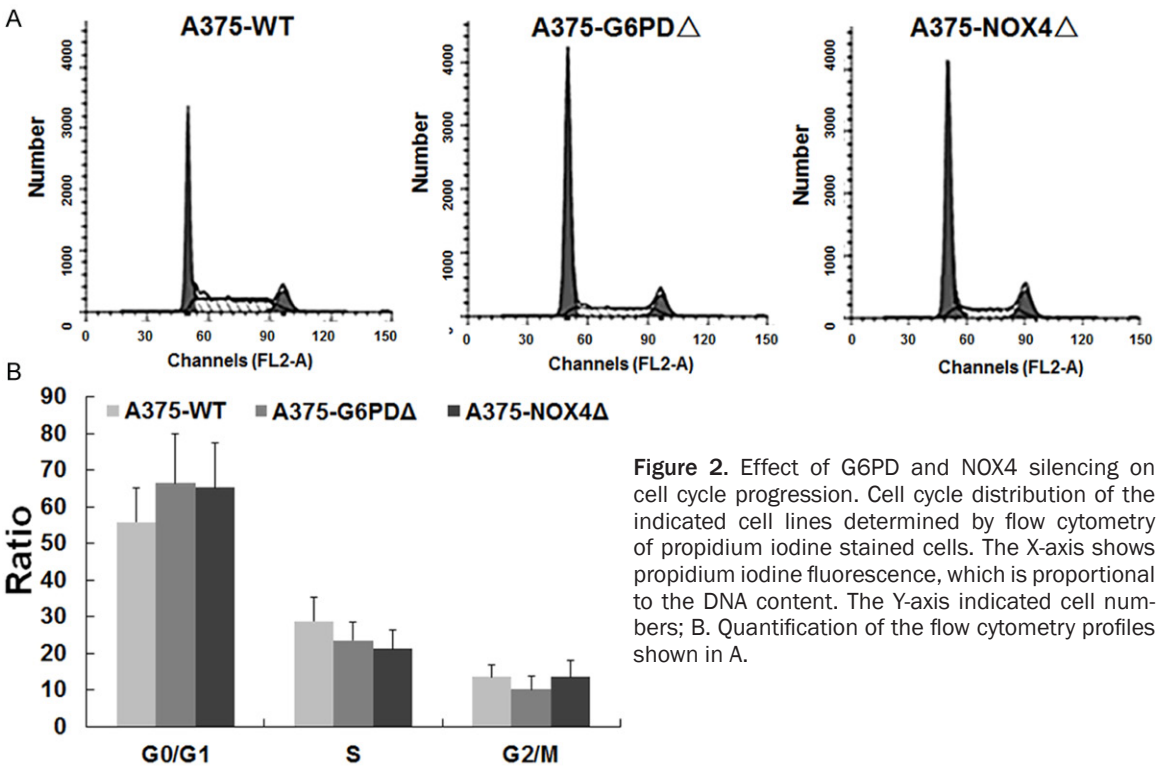

Figure 2. Effect of G6PD and NOX4 silencing on cell cycle progression. Cell cycle distribution of the indicated cell lines determined by flow cytometry of propidium iodine stained cells. The X-axis shows propidium iodine fluorescence, which is proportional to the DNA content. The Y-axis indicated cell numbers; B. Quantification of the flow cytometry profiles shown in A.

human melanoma cell lines A375, M21 and SK-mel-28. HEMs are pigment-producing cells isolated from the basal layer of the epidermis, while A375, M21 and SK-mel-28 are amelanot-

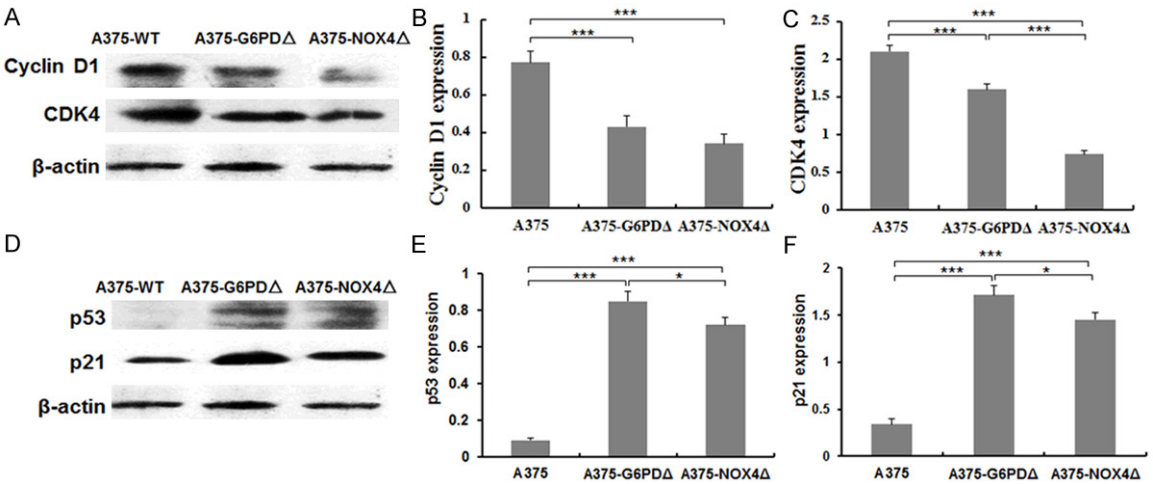

Figure 3. Levels of cyclin D1, CDK4, p53 and p21 protein expression in A375 derived cell lines. A. Cyclin D1 and CDK4 protein expression in the indicated cell lines was determined by Western blotting. β-actin levels are shown for reference. B, C. Quantification of the blots in A. D. p53 and p21 protein expression in the indicated cell lines determined by Western blotting. β-actin is shown as a reference. E, F. Quantification of the blots shown in D. *P < 0.05, ***P < 0.001.

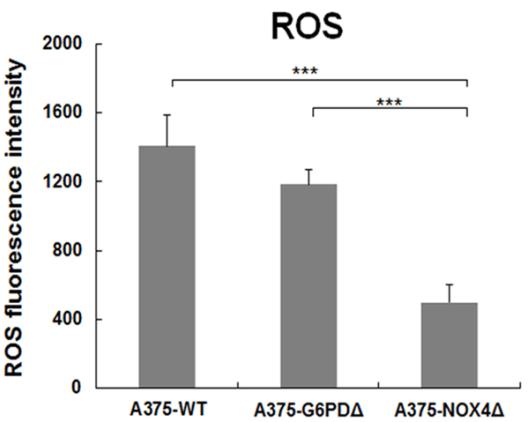

Figure 4. ROS levels in A375-WT, A375-G6PDΔ and A375-NOX4Δ cells. ROS levels were determined in the indicated cell lines by measuring DHE fluorescence during flow cytometry. The graph displays average results from three independent experiments and error bars represent the SD. ***P < 0.001.

ic melanoma cell lines. The basal mRNA levels of both *G6PD* and *NOX4* were significantly lower in HEMs, M21 and SK-mel-28 cells compared to A375 cells (**Figure 1A**). The different expression levels were further confirmed by Western blotting, which again showed considerably lower protein levels of both factors in HEMs, M21 and SK-mel-28 compared to A375 cells (**Figure 1B**). In A375 cells, the mRNA level of G6PD was slightly lower than that of NOX4, while the opposite pattern was observed at the protein level. Thus, post-transcriptional or post-translational mechanisms appear to be involved in the expression of these products in A375 cells. In order to determine whether the differences in protein expression were reflected in the level of enzyme activity, *in vitro* enzyme assays were carried out, and similar pattern expressions were observed (**Figure 1C**). Next, we used A375 cells as the study subject.

Effect of G6PD and NOX4 silencing on cell cycle progression and ROS production

In order to investigate the cellular consequences of inhibiting G6PD expression, we employed parental A375 cells (A375-WT) as well as derivatives in which G6PD or NOX4 were silenced (A375-G6PDΔ and A375-NOX4Δ, respectively). Flow cytometry of propidium iodine stained cells showed that silencing of G6PD or NOX4 led to a cell cycle delay in G1 (66.3% and 65.2% versus 55.8% in wild-type A375 cells) (**Figure 2A**, **2B**). The increase in the G1 phase occurred at the expense of the S phase population, which decreased from 28.8% in wild-type cells to 23.5% and 21.3% in A375-G6PDΔ and A375-NOX4Δ cells, respectively. The fraction of cells in G2 was also reduced by G6PD silencing but not by silencing of NOX4 (**Figure 2B**). These finding demonstrate that reduced levels of G6PD and NOX4 in A375 cells induce a cell cycle delay at the G1/S border.

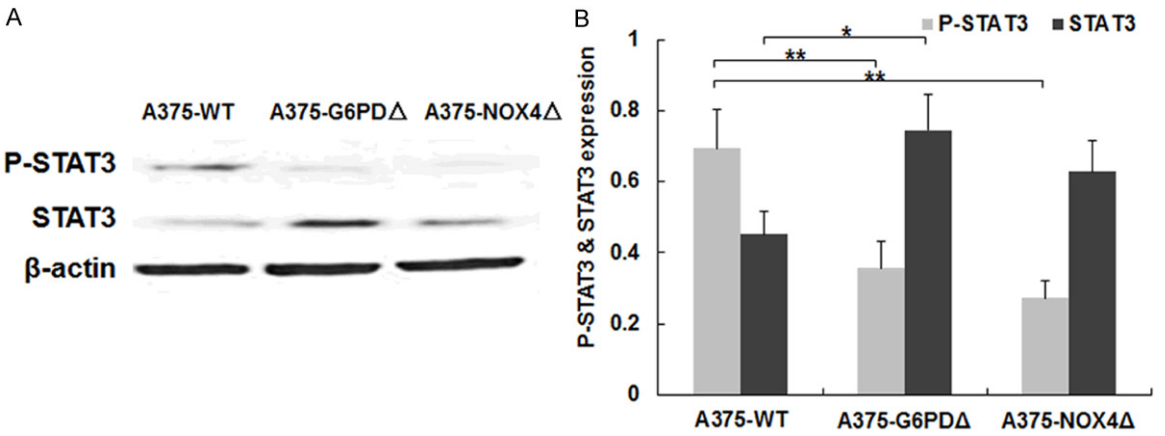

Figure 5. Levels of STAT3 and phosphorylated STAT3 in A375 derived cell lines. A. Levels of the indicated proteins were determined by Western blotting of cell lysate from the indicated cell lines. β-actin signals are shown for reference. B. Quantification of STAT3 and phospho-STAT3 levels in the indicated cell lines. The graph represents results from three independent experiments. *P < 0.05, **P < 0.01.

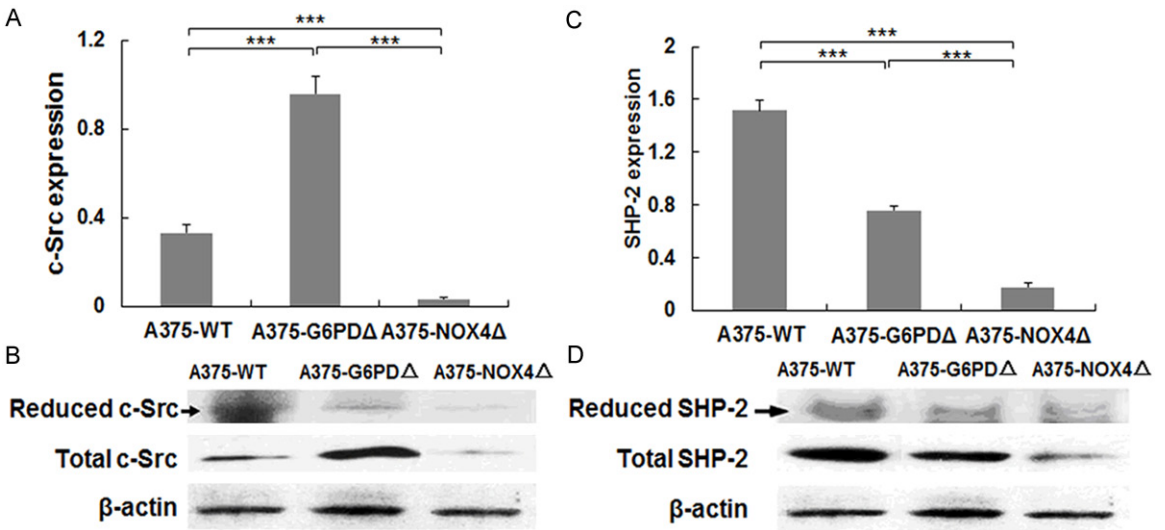

Figure 6. Levels of c-Src and SHP-2 in A375 cells. A, C. The levels of reduced c-Src and SHP-2 and total c-Src and SHP-2 protein expression in the indicated cell lines were determined by immunoblotting. The signals for β-actin are shown for reference. B, D, Quantification of the blots in A and C. Bar graphs show averages of 3 independent experiments with standard error bars. ***P < 0.001.

To investigate further this response, we examined the expression patterns of several important cell cycle regulatory proteins in the various cell lines. Relative quantification of immunoblots revealed a significant downregulation of cyclin D1 (44.1%, $P = 0.003$) and its interacting kinase CDK4 (23.9%, $P = 0.002$) upon silencing of G6PD. In contrast, there were significant increases in p53 (8.32 times, $P < 0.01$) and p21 (4.03 times, $P < 0.01$) (**Figure 3A**, **3D**). Qualitatively similar responses were seen in NOX4 silenced cells with cyclin D1 and CDK4 expression decreasing by 55.7% ($P = 0.0004$) and 64.8% ($P = 0.01$), respectively. Instead, p53 levels increased 6.89 times ($P < 0.01$), whereas p21 rose 3.27 times ($P < 0.01$) (**Figure 3B**, **3C**, **3E**, **3F**). The significance of the differences in the expression of these critical regulatory proteins was assessed by population variance analysis with the following results: Cyclin D1: F = 17.251, $P = 0.0003$; CDK4: F = 19.281, $P = 0.0023$; p53: F = 111.94, $P < 0.01$; p21: F = 82.224, $P < 0.01$.

Since both G6PD and NOX4 were shown to influence the cellular redox state, ROS levels

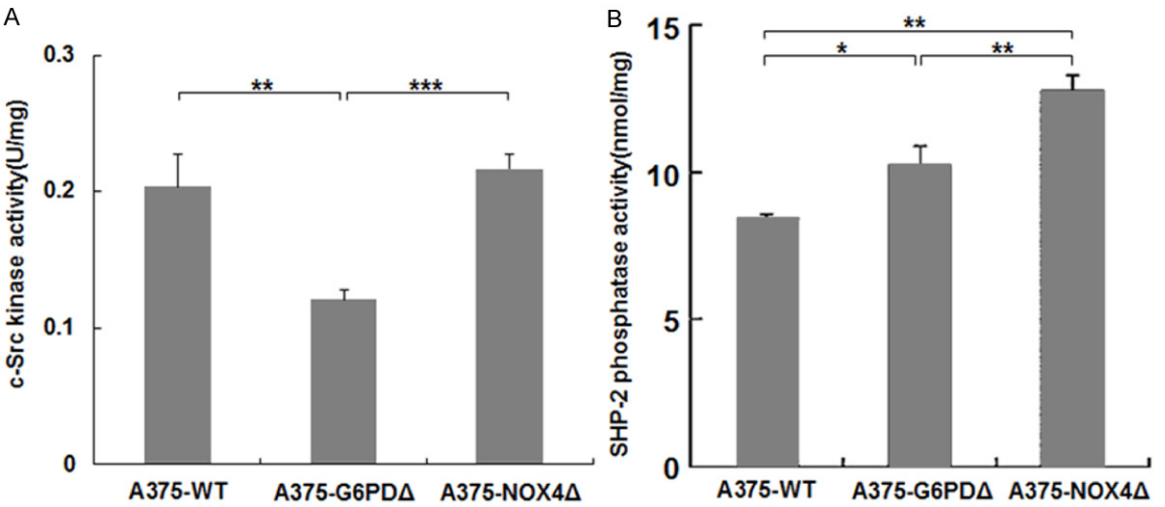

Figure 7. In vitro activity of c-Src and SHP2 in the indicated cell lines A, B. c-SRC and SHP2 were immunopurified from lysates of A375 derivative cell lines and employed in a colorimetric activity assay. The graph represents average measurements from three independent experiments, and error bars represent the SD. *P < 0.05, **P < 0.01, ***P < 0.001.

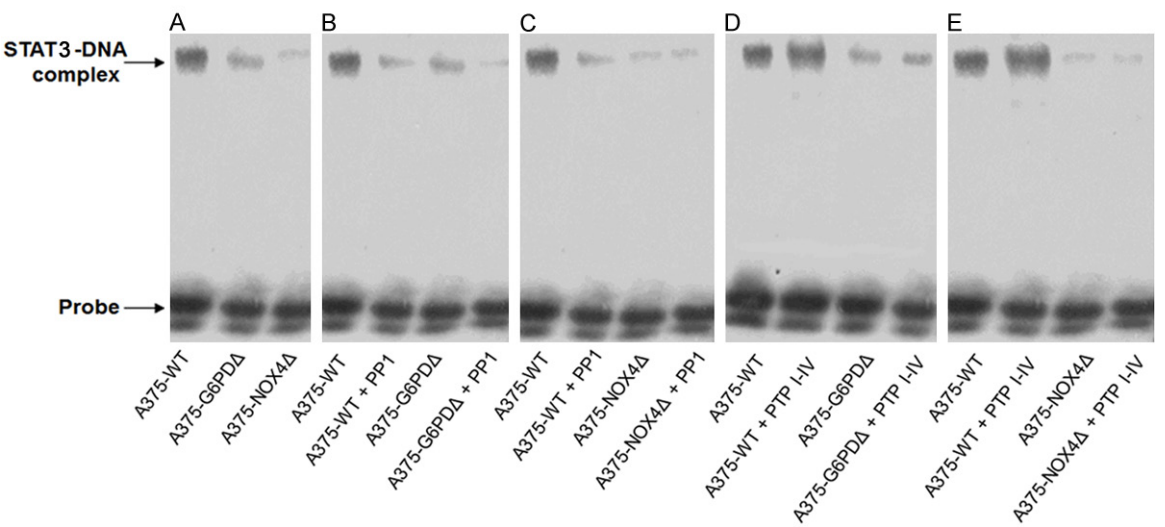

Figure 8. STAT3 in vitro DNA binding activity determined by EMSA. A. DNA binding activity of STAT3 as determined by EMSA with nuclear extract prepared from the indicated A375 derivative cell lines. B, C, Effect of the SRC inhibitor PP1 (10 μM) on STAT3 in vitro DNA binding activity in the indicated cell lines. D, E, Effect of the PTP inhibitor IV (5 μM) on STAT3 in vitro DNA binding activity in the indicated cell lines.

were determined in A375-WT, A375-G6PDΔ and A375-NOX4Δ cells. Reductions in ROS levels were detected in NOX4Δ cells relative to A375-WT (64.5%, t = 7.686, *P* = 0.002) and A375-G6PDΔ (57.83%, t = 9.102, *P* = 0.001) cells (**Figure 4**). In contrast, there was no significant difference in ROS levels between A375-WT and A375-G6PDΔ cells (t = 1.945, *P* = 0.124, **Figure 4**).

Effect of G6PD and NOX4 silencing on STAT3 expression

Since ROS can activate STAT3, it was of interest to determine the effect of suppressing G6PD and NOX4 on STAT3 activity. Compared to wild-type A375 cells, A375-G6PDΔ cells showed significantly lower levels of phospho-STAT3. STAT3 levels were significantly higher in A375-G6PDΔ

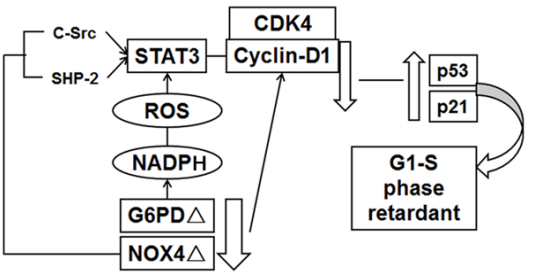

Figure 9. General model of G6PD-NOX4-NADPH-ROS-c-SRC/SHP2-START3 pathways in melanoma A375 (see Discussion for details).

cells (+34.0%, $P = 0.034$) relative to A375-WT cells (**Figure 5A**). However, the active species phospho-STAT3 was downregulated by 52.6% ($P < 0.01$) (**Figure 5A**). A qualitatively similar pattern was observed in A375- NOX4Δcells. (**Figure 5A**, **5B**).

G6PDΔ and NOX4Δ can alter STAT3 activity by influencing its phosphorylation status. In order to determine whether the activity, expression and redox states of c-Src and SHP2 might be regulated by phosphorylation, we tested the reduced state of c-Src and SHP2 and total c-Src and SHP2 protein levels in different A375 cell lines. C-Src levels were 2.9 times higher in A375-G6PDΔ cells (t = 14.918, $P = 0.001$) than in parental A375 cells, but decreased 89.46% in A375-NOX4Δ cells (t = 14.55, $P = 0.004$). Expression of SHP2 was lower in both A375-G6PDΔ (-50.1%, t = 14.91, $P = 0.001$) and A375-NOX4Δ cells (88.5%, t = 26.91, $P = 0.0$), respectively. In contrast, reduced c-Src and SHP-2 proteins decreased successively in A375-G6PDΔ and A375-NOX4Δ cells (**Figure 6**).

The *in vitro* activity of c-Src and SHP2 was examined in the various cell lines using colorimetric assays. c-Src activity was 41.2% (t = 5.740, $P = 0.019$) lower in A375-G6PDΔ versus A375 cells, while no significant change was seen in A375-NOX4Δ cells, (t = 0.853, $P = 0.460$). c-Src activity in A375-NOX4Δ was 1.8 times higher than in A375-G6PDΔ cells (t = 12.53, $P = 0.000$) (**Figure 7A**). Compared with A375-WT, SHP2 activity was 17.30% (t = 4.761, $P = 0.028$) and 33.8% (t = 14.5, $P = 0.004$) higher in A375-G6PDΔ and A375-NOX4Δ cells, respectively. A375-NOX4Δ had 19.9% (t = 5.415, $P = 0.006$) lower SHP2 activity than A375-G6PDΔ cells (**Figure 7B**).

Finally, the *in vitro* DNA binding activity of STAT3 was assessed in an electrophoretic mobility shift assay (EMSA). Nuclear proteins were prepared from A375, A375-G6PDΔ and A375-NOX4Δ cells and employed in EMSAs with a double stranded oligonucleotide containing a canonical STAT3 binding site. The assay showed that STAT3 DNA-binding activity was substantially lower in A375-G6PDΔ and A375-NOX4Δ cells relative to wild-type A375 cells with the difference being more pronounced for A375-NOX4Δ cells (**Figure 8A**).

Treatment of A375-WT cells with the SRC inhibitor PP1 resulted in suppression of STAT3 DNA binding activity. Some minor suppression was also seen in A375-G6PDΔ and A375-NOX4Δ cells (**Figure 8B**, **8C**). Substantial upregulation of STAT3 DNA binding activity was observed in nuclear lysate of A375-WT cells treated with the SHP2 inhibitor PTP inhibitor IV, whereas no effect was detected in the A375-G6PDΔ and A375-NOX4Δ cell lines (**Figure 8D**, **8E**).

Discussion

G6PD is a key metabolic enzyme that catalyses the first step of the pentose phosphate pathway. G6PD has been reported to be highly expressed and active in various human tumors such as melanoma, breast cancer, ovarian cancer, prostate cancer and lung cancer, indicating that G6PD might play an important role in cancer [14]. STAT3 was also linked to carcinogenesis and tumor development [15, 16]. Yin et al. showed that the inhibition of STAT3 expression reduces melanoma growth in the mouse [17]. Furthermore, Tworkoski et al. reported that human epidermal growth factor receptor 3 (HER3) and insulin-like growth factor 1 receptor (IGFIR) function in melanoma development through the STAT3 pathway [18]. In this study, the G6PD-related mechanism and cell response has been examined in A375 melanoma cells. By investigating the cell cycle distribution of G6PD and NOX4 in silencing A375 cells, we discovered that deficiency in G6PD and NOX4 induced a G1/S arrest. Further studies revealed decreased levels of the positive cell cycle regulators cyclin D1 and CDK4 along with increased levels of the negative regulator p53 and p21, suggesting that G6PD and NOX4 knockdown inhibits melanoma cell division and proliferation by affecting these cell cycle proteins. The modified A375 cells are halted in the G1 phase presumably to induce programmed cell death.

The tumor suppressor p53 has also been implicated as an upstream regulator of STAT3, cyclin D1 and CDK4 [19]. We found reduced DNA binding activity of STAT3 in the A375-G6PDΔ and A375-NOX4Δ cells compared to A375-WT. The inhibition of STAT3 might be related to changes in the expression and activity of c-SRC and SHP2 upon silencing of G6PD and NOX4. Additionally, as previously reported, increased ROS levels in A375 cells activate STAT3 [20, 21]. For example, IL6 can upregulate STAT3 in A375 cells by inducing ROS, although the exact molecular mechanisms remain unclear. c-SRC kinase regulates the JAK and AKT pathways, stimulates STAT3 nuclear import and directly phosphorylates tyr 705 of STAT3 [22]. Thus, c-SRC-mediated phosphorylation may link ROS to STAT3 activation.

SHP2 is likewise controlled by ROS and may regulate STAT3 activity by dephosphorylating the transcription factor. In wild-type A375 cells treated with PTP inhibitor IV, STAT3 DNA binding activity may be increased as a consequence of reduced phosphorylation of STAT3 on serine 727 due to inhibition of SHP2. In A375-NOX4Δ cells, STAT3 phosphorylation on tyrosine 705 is low, apparently as a result of low c-SRC activity. Thus, despite a high level of serine 727 phosphorylation, STAT3 DNA binding activity remains unaffected in A375-NOX4Δ cells. These data suggest that in the A375-G6PDΔ and A375-NOX4Δ cells, the DNA-binding activity of STAT3 is primarily regulated by c-SRC, while SHP2 may fine-tune the activity.

In summary, our data suggest a novel pathway for controlling STAT3 activity in melanoma cells that involves modulation of c-SRC and SHP2 downstream of G6PD and NOX4-mediated redox signaling (**Figure 9**).

After G6PD and NOX4 knock down, melanoma A375 cells showed G1 and S phase retardant and proliferation inhibition by downregulating the expression of cyclin D1 and CDK4, upregulating p53 and p21 expression. It is an important molecular mechanism that the activity of STAT3 combined with DNA decreased, which lead to inhibition of A375 cell proliferation. In human melanoma A375 cells, the functional activity of STAT3 is mainly regulated by its upstream gene c-Src and SHP-2; In G6PD deficient A375 cells, STAT3 activity is mainly regulated by c-Src; In A375 knocked down cells; NOX4 can inhibit c-Src and SHP-2 on the regulation of STAT3 activity.

Acknowledgements

This work was supported by a grant from the National Natural Science Foundation of China (no. 81160246 and 81460421) and Yunnan Provincial Science and Technology Foundation (no. 2013FB102).

Disclosure of conflict of interest

No competing financial conflicts exist.

Address correspondence to: Yuechun Zhu, Department of Biochemistry and Molecular Biology, Kunming Medical University, No. 191, West Renming Road, Kunming 650500, China. Tel: +86-15368205856; Fax: +86-0871-65922854; E-mail: zhuyuechunbm@163.com

References

[1] Wadasadawala T, Trivedi S, Gupta T, Epari S and Jalali R. The diagnostic dilemma of primary central nervous system melanoma. J Clin Neurosci 2010; 17: 1014-1017.

[2] Xie Q, Lan G, Zhou Y, Huang J, Liang Y, Zheng W, Fu X, Fan C and Chen T. Strategy to enhance the anticancer efficacy of X-ray radiotherapy in melanoma cells by platinum complexes, the role of ROS-mediated signaling pathways. Cancer Lett 2014; 354: 58-67.

[3] Pandolfi PP, Sonati F, Rivi R, Mason P, Grosveld F and Luzzatto L. Targeted disruption of the housekeeping gene encoding glucose 6-phosphate dehydrogenase (G6PD): G6PD is dispensable for pentose synthesis but essential for defense against oxidative stress. EMBO J 1995; 14: 5209-5215.

[4] Love NR, Ziegler M, Chen Y and Amaya E. Carbohydrate metabolism during vertebrate appendage regeneration: what is its role? How is it regulated?: A postulation that regenerating vertebrate appendages facilitate glycolytic and pentose phosphate pathways to fuel macromolecule biosynthesis. Bioessays 2014; 36: 27-33.

[5] Vaca G, Arambula E and Esparza A. Molecular heterogeneity of glucose-6-phosphate dehydrogenase deficiency in Mexico: overall results of a 7-year project. Blood Cells Mol Dis 2002; 28: 436-444.

[6] Yan T, Cai R, Mo O, Zhu D, Ouyang H, Huang L, Zhao M, Huang F, Li L, Liang X and Xu X. Incidence and complete molecular characterization of glucose-6-phosphate dehydrogenase

deficiency in the Guangxi Zhuang autonomous region of southern China: description of four novel mutations. Haematologica 2006; 91: 1321-1328.

[7] Hu T, Zhang C, Tang Q, Su Y, Li B, Chen L, Zhang Z, Cai T and Zhu Y. Variant G6PD levels promote tumor cell proliferation or apoptosis via the STAT3/5 pathway in the human melanoma xenograft mouse model. BMC Cancer 2013; 13: 251.

[8] Cheng G, Cao Z, Xu X, van Meir EG and Lambeth JD. Homologs of gp91phox: cloning and tissue expression of Nox3, Nox4, and Nox5. Gene 2001; 269: 131-140.

[9] Spencer NY, Yan Z, Boudreau RL, Zhang Y, Luo M, Li Q, Tian X, Shah AM, Davisson RL, Davidson B, Banfi B and Engelhardt JF. Control of hepatic nuclear superoxide production by glucose 6-phosphate dehydrogenase and NADPH oxidase-4. J Biol Chem 2011; 286: 8977-8987.

[10] Chong ZZ and Maiese K. The Src homology 2 domain tyrosine phosphatases SHP-1 and SHP-2: diversified control of cell growth, inflammation, and injury. Histol Histopathol 2007; 22: 1251-1267.

[11] Kleniewska P, Piechota A, Skibska B and Goraca A. The NADPH oxidase family and its inhibitors. Arch Immunol Ther Exp (Warsz) 2012; 60: 277-294.

[12] Liu L, Nam S, Tian Y, Yang F, Wu J, Wang Y, Scuto A, Polychronopoulos P, Magiatis P, Skaltsounis L and Jove R. 6-Bromoindirubin-3'-oxime inhibits JAK/STAT3 signaling and induces apoptosis of human melanoma cells. Cancer Res 2011; 71: 3972-3979.

[13] Nam S, Xie J, Perkins A, Ma Y, Yang F, Wu J, Wang Y, Xu RZ, Huang W, Horne DA and Jove R. Novel synthetic derivatives of the natural product berbamine inhibit Jak2/Stat3 signaling and induce apoptosis of human melanoma cells. Mol Oncol 2012; 6: 484-493.

[14] Zhang C, Zhang Z, Zhu Y and Qin S. Glucose-6-phosphate dehydrogenase: a biomarker and potential therapeutic target for cancer. Anticancer Agents Med Chem 2014; 14: 280-289.

[15] Nguyen AV, Wu YY, Liu Q, Wang D, Nguyen S, Loh R, Pang J, Friedman K, Orlofsky A, Augenlicht L, Pollard JW and Lin EY. STAT3 in epithelial cells regulates inflammation and tumor progression to malignant state in colon. Neoplasia 2013; 15: 998-1008.

[16] Haricharan S and Li Y. STAT signaling in mammary gland differentiation, cell survival and tumorigenesis. Mol Cell Endocrinol 2014; 382: 560-569.

[17] Yin D, Li Y, Lin H, Guo B, Du Y, Li X, Jia H, Zhao X, Tang J and Zhang L. Functional graphene oxide as a plasmid-based Stat3 siRNA carrier inhibits mouse malignant melanoma growth in vivo. Nanotechnology 2013; 24: 105102.

[18] Tworkoski K, Singhal G, Szpakowski S, Zito CI, Bacchiocchi A, Muthusamy V, Bosenberg M, Krauthammer M, Halaban R and Stern DF. Phosphoproteomic screen identifies potential therapeutic targets in melanoma. Mol Cancer Res 2011; 9: 801-812.

[19] Niu G, Wright KL, Ma Y, Wright GM, Huang M, Irby R, Briggs J, Karras J, Cress WD, Pardoll D, Jove R, Chen J and Yu H. Role of Stat3 in regulating p53 expression and function. Mol Cell Biol 2005; 25: 7432-7440.

[20] Bill MA, Bakan C, Benson DM Jr, Fuchs J, Young G and Lesinski GB. Curcumin induces proapoptotic effects against human melanoma cells and modulates the cellular response to immunotherapeutic cytokines. Mol Cancer Ther 2009; 8: 2726-2735.

[21] Chen CY, Chen YK, Wang JJ, Hsu CC, Tsai FY, Sung PJ, Lin HC, Chang LS and Hu WP. DC-81-enediyne induces apoptosis of human melanoma A375 cells: involvement of the ROS, p38 MAPK, and AP-1 signaling pathways. Cell Biol Toxicol 2013; 29: 85-99.

[22] Soldaini E, John S, Moro S, Bollenbacher J, Schindler U and Leonard WJ. DNA binding site selection of dimeric and tetrameric Stat5 proteins reveals a large repertoire of divergent tetrameric Stat5a binding sites. Mol Cell Biol 2000; 20: 389-401.